An investigation into the effects of ink formulations of semi-solid extrusion 3D printing on the performance of the printed solid dosage forms

Bin Zhang[a,b]†, Peter Belton[c], Xin Yi Teoh[d], Andrew Gleadall[e], Richard Bibb[f], and Sheng Qi[a] †

[a]School of Pharmacy, University of East Anglia, Norwich, UK

[b]Department of Mechanical and Aerospace Engineering, Brunel University London, London, UK

[c]School of Chemistry, University of East Anglia, Norwich, UK

[d]School of Pharmaceutical Sciences, Universiti Sains Malaysia, Penang, Malaysia

[e]Wolfson School of Mechanical, Electrical and Manufacturing Engineering, Loughborough University, Loughborough, UK

[f] Nottingham School of Art & Design, Nottingham Trent University, UK

† Corresponding author. E-mail: sheng.qi@uea.ac.uk ; bin.zhang@brunel.ac.uk

Abstract

Semi-solid extrusion (SSE) 3D printing has recently attracted increased attention for its pharmaceutical application as a potential method for small-batch manufacturing of personalised solid dosage forms. It has the advantage of allowing ambient temperature printing, which is especially beneficial for the 3D printing of thermosensitive drugs. In this study, the effects of polymeric compositions (single hydroxypropyl methylcellulose (HPMC) system and binary HPMC+ Polyvinylpyrrolidone (PVP) system), disintegrant (silicon oxide (SiO_2)), and active pharmaceutical ingredients (tranexamic acid (TXA) and paracetamol (PAC)) on the printability of semisolid inks and the qualities of SSE printed drug-loaded tablets were investigated. Printability is defined by the suitability of the material for the process in terms of its physical properties during extrusions and post-extrusion, including rheology, solidification time, avoiding slumping, etc. The rheological properties of the inks were investigated as a function of polymeric compositions and drug concentrations and further correlated with the printability of the inks. The SSE 3D printed tablets were subjected to a series of physicochemical properties characterisations and *in vitro* drug release performance evaluations. The results indicated that an addition of SiO_2 would improve 3D printing shape fidelity (e.g., pore area and porosity) by altering the ink rheology. The pores of HPMC+PVP+5PAC prints completely disappeared after 12 hours of drying (pore area = 0 mm^2). An addition of SiO_2 significantly improved the pore area of the prints which are 3.5±0.1 mm^2. It was noted that the drug release profile of PAC significantly increased ($p<0.05$) when additive SiO_2 was incorporated in the formulation. This could be due to a significantly higher porosity of HPMC+PVP+SiO_2+PAC (70.3±0.2%) compared to HPMC+PVP+PAC (47.6±2.1%). It was also likely that SiO_2 acted as a

disintegrant and speeding up the drug release process. Besides, the incorporation of APIs with different aqueous solubilities, as well as levels of interaction with the polymeric system showed significant impacts on the structural fidelity and subsequently the drug release performance of 3D printed tablets.

Keywords: Semi-solid extrusion 3D printing, drug delivery, personalised medicine, disintegrant, ink rheology, printability, shape fidelity, *in vitro* drug release.

1 Introduction

3D printing is attracting increasing attention in the pharmaceutical science community due to its flexibility and customizability potential for personalised medicine when compared to traditional pharmaceutical mass manufacturing techniques (1, 2). In recent years, several 3D printing techniques have been investigated for their potential pharmaceutical applications, including stereolithography (3, 4), selective laser sintering (5), inkjet printing (6, 7), and material-extrusion 3D printing (8-11). Among these, thermal-based 3D printing processes, including fused deposition modelling (FDM), direct powder extrusion and droplet deposition-based 3D printing (12-16), are widely researched. However, thermal-based 3D printing requires the active pharmaceutical ingredient (API) to go through at least one (and two for FDM) thermal processes (heating above melting point to create the material filament by extrusion and subsequent reheating during printing), which could cause drug thermal degradation and is not suitable for thermosensitive drugs. Several modifications have been attempted to reduce the thermal stress associated with thermal-based 3D printing methods, such as adding plasticisers to the formula to lower the melting/glass transition temperature of the bulk polymers, thus lowering the printing temperature required to process the material (8, 17-21), but none of these can completely eliminate the effects of heat during printing.

Semi-solid extrusion (SSE) 3D printing is a 3D printing technology which extrudes semi-solid materials such as pastes and gels through a defined size nozzle to create a new structure after solidification (e.g., tablets). Compared to thermal-based 3D printing methods, SSE 3D printing can operate under a heat-free condition as the printing solely

relies on the extrusion of viscoelastic semi-solid inks through a nozzle with a displacement-controlled driving mechanism (22-25). The rheological and mechanical properties of the ink formulas are critical for successful SSE 3D printing (26-28). The formulated ink is technically a slurry (with solid contents) or a gel (soluble ingredients with hydrated polymer network) (23, 29-32). It is commonly recognised in the literature that in order to achieve high geometrical fidelity using SSE 3D printing, meaning accurately reproducing the original CAD design, certain characteristics are required. These are that the ink needs to exhibit non-Newtonian properties and shear-thinning behaviour (i.e. reduction in viscosity with applied shear stress) to generate continuous flow during extrusion (24, 33, 34). If the ink viscosity is too low, discontinuous droplets or overflooding and deformation of filaments would occur, while nozzle clogging happens, if the ink viscosity is too high (35-37). Thickening additives often have to be used to adjust the ink viscosity (38-40).

A wide range of pharmaceutical applications of SSE 3D printing have been demonstrated in the literature, including chewable and fast-disintegrating dosage forms as well as polypills (41, 42), which have been developed for paediatric patients, patients with dysphagia and patients with high pill burdens. These published works highlighted the potential of SSE as a manufacturing method to produce personalised medicines for targeted patient groups. Whilst SSE 3D printing has advantages, it still remains in the research and development stage, and there are presently the limitations of (1) suitable ink formulation for 3D printing, (2) lack of understanding of the influences of ingredients in the ink formula on drug release. Thus, in order to translate the technology

to clinical practice, a fundamental understanding of the key principles of optimising the printability of SSE inks is needed to guide new product development (22, 27, 43).

Commonly used excipient/additive of pharmaceutical products i.e. HPMC, PVP and SiO_2 (44-46) were selected in this study. As a ramification of our previous study where HPMC-PVP was identified as an ideal excipient combination in semisolid extrusion-based 3D printing (22), therefore, this study aims to investigate the effect of additive and APIs incorporation on the printability and drug release performance of 3D printed tablets. In this study, additive SiO_2 as the disintegrant and two APIs with different levels of water solubilities (i.e., tranexamic acid (TXA) and paracetamol (PAC)) were incorporated into the ink to observe the changes in ink properties. Subsequently, an attempt to establish the relationship between ink properties, shape fidelity of printed tablets and *in vitro* drug release behaviours was conducted.

2 Materials and methods

2.1 Materials

Hydroxypropyl methylcellulose (HPMC) (METOLOSE® SR 90SH-4000, Mw 270,000 g/mol) was donated by Shin-Etsu Chemical Co. Ltd. (Tokyo, Japan). Polyvinylpyrrolidone (PVP, Mw 50,000 g/mol) and silicon oxide (SiO_2, 50 µm) were received as generous gifts from BASF (Ludwigshafen, Germany) and Evonik (Darmstadt, Germany) respectively. Tranexamic acid (TXA, Mw 157.21 g/mol) and paracetamol (PAC, Mw 151 g/mol) were purchased from Molekula (Darlington, UK). Salicylaldehyde (SA), used as an agent for UV detection of the TXA, was purchased from Sigma-Aldrich (St. Louis, Missouri, United States). Polymer and drug chemical structures is shown in **Figure 1**.

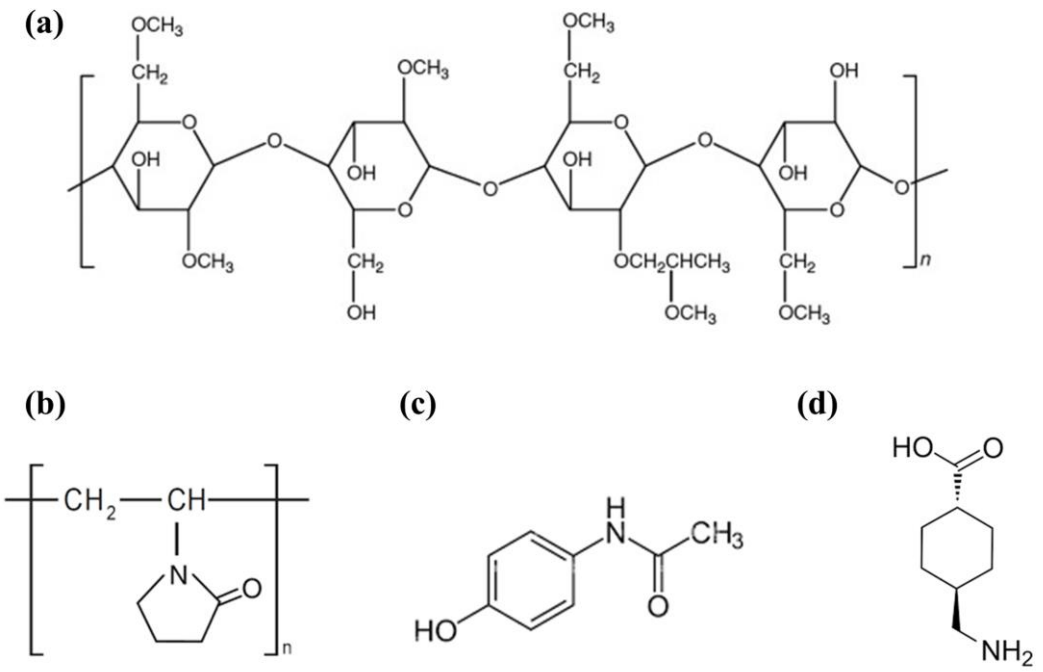

Figure 1. Polymer and drug chemical structures (a) HPMC, (b) PVP, (c) PAC and (d) TXA.

2.2 Ink formulation

Both TXA- and PAC-loaded inks were prepared by dissolving the drug (at drug concentrations of TXA 5-30% w/w, and 5% w/w PAC) in 20g deionised water at ambient temperature (circa 21 °C). Subsequently, HPMC and PVP were respectively added at 15-20% w/w to be dispersed to form a homogenous semi-solid mass under mechanical stirring. SiO_2 powder (with a mean particle size of 50 μm) was added to the HPMC/PVP drug-loaded inks as a disintegrant additive. The ink preparation protocol is described in **Figure S1**, and the compositions of the ink formulated are listed in **Table 1**.

87 **Table 1**. List of investigated inks and their corresponding ingredients*

	Polymer	**Additive**		**API**	
Ink name	HPMC (%w/w)	PVP (%w/w)	SiO_2 (%w/w)	TXA (%w/w)	PAC (%w/w)
Influence of additive/excipient					
15HPMC	15	-	-	-	-
30HPMC	30	-	-	-	-
35HPMC	35	-	-	-	-
PVP	-	20	-	-	-
HPMC+PVP	15	20	-	-	-
HPMC+PVP+SiO_2	15	20	8	-	-
Influence of API					
HPMC+15TXA	15	-	-	15	-
HPMC+PVP+15TXA	15	20	-	15	-
HPMC+PVP+SiO_2+15TXA	15	20	8	15	-
HPMC+5PAC	15	-	-	-	5
HPMC+PVP+5PAC	15	20	-	-	5
HPMC+PVP+SiO_2+5PAC	15	20	8	-	5
Influence of API concentration					
HPMC+PVP	15	20	-	-	-
HPMC+PVP+5TXA	15	20	-	5	-
HPMC+PVP+15TXA	15	20	-	15	-
HPMC+PVP+30TXA	15	20	-	30	-

88 *All % w/w is calculated by the weight of each ingredient to the weight of deionised water.

2.3 Design 3D constructs

3D constructs of the drug-loaded prints with different layer thicknesses and infill were designed to examine the geometry effect on drug release. The detailed design parameters of the constructs are summarised in **Table 2**. The designs can be divided into two approaches: (1) 3D tablet lattice with two options for the number of layers (4 and 14) whilst the pore width and filament width were kept constant; (2) 3D constructs with a fixed number of layers (14) but with various infill densities by varying the pore width at 1 mm or 2 mm.

Table 2. The CAD parameters of the 3D constructs designs of drug-loaded prints.

	Tablet width (mm)	**Tablet length (mm)**	**Tablet thickness (mm)**	**Filament width (mm)**	**Pore width (mm)**
Influence of layer number					
HPMC+PVP+5TXA_4layer	20	20	1	0.4	2
HPMC+PVP+15TXA_4layer	20	20	1	0.4	2
HPMC+PVP+5TXA_14layer	20	20	3	0.4	2
HPMC+PVP+15TXA_14layer	20	20	3	0.4	2
Influence of infill (%)					
HPMC+PVP+5TXA_25%infill	20	20	3	0.4	2
HPMC+PVP+15TXA_25%infill	20	20	3	0.4	2
HPMC+PVP+5TXA_50%infill	20	20	3	0.4	1
HPMC+PVP+15TXA_50%infill	20	20	3	0.4	1

2.4 SSE 3D printing

An SSE 3D printer (BioX, Cellink Life Sciences, Gothenburg, Sweden) was used to fabricate the drug-free and drug-loaded 3D constructs. The G-code of the design was generated in accordance with the predesigned CAD model. All prints were performed at ambient temperature (circa 21 °C), and the printing nozzle and printing platform were not heated. The ink materials were extruded from a 22 Gauge nozzle, which is equivalent to an internal diameter (ID) of 413 µm. The extrusion rate (1–5 µL/s) and printing speed (5–20 mm/s) were optimised to obtain a filament diameter close to the nozzle diameter upon printing. Each layer was comprised of parallel filaments with an average width of circa 413 µm.

2.5 Rheological measurements

Rheological measurements of the inks were conducted at ambient temperature using a rheometer (Discovery HR30, TA Instruments, New Castle, Delaware, USA) with a cone-plate geometry. Continuous flow ramps were performed by varying the shear rate from 0.1 to 100 s^{-1}. Three replicates were measured for each ink formula.

2.6 Shape fidelity and surface morphology analysis of the prints

A FDSC196 polarised light microscope (PLM) (Linkam Scientific, Surrey, UK) was used to detect drug crystals through birefringent observation as an indication of the changes in drug solubility limit in the inks after the addition of HPMC and PVP (as the addition of HPMC and PVP may affect the aqueous solubility of the drug).

The microscope was used to inspect the printed constructs. The pore areas of the printed structures were measured using Image J software (Version 1.8.0, Bethesda, Maryland, USA). The measurements were repeated at three different prints and three pores were measured for each print. The dimensional data were plotted using Origin software

(Version 2018, Northampton, Massachusetts, USA). Error bars represent the mean ± standard deviation. The pore area of 3D printed tablets was later compared with the theoretical value. A theoretical value of pore area at 4 mm^2 was identified as expressed as the square of pore width. Thus, the pore area under-sizing (%) is calculated in Eq. (1).

$$\text{Pore area under} - \text{sizing (\%)} = \frac{\mathrm{A_{theory}} - \mathrm{A_{printing}}}{\mathrm{A_{theory}}} \qquad (1)$$

where $\mathrm{A_{theory}}$ is theoretical pore area, $\mathrm{A_{printing}}$ is the pore area at n^{th} mins after printing. Assuming SSE 3D printed samples are dried, experimental solid volume ($\mathrm{V_{exp}}$) of the printed constructs was calculated based on their actual weight ($\mathrm{M_{exp}}$) divided by their density (ρ_{exp}), as shown in Eq. (2).

$$\mathrm{V_{exp}} = \frac{\mathrm{M_{exp}}}{\rho_{exp}} \qquad (2)$$

Considering the samples were printed with HPMC, PVP and SiO_2 mixed with API (i.e., TXA or PAC), the density of SSE 3D printed samples was calculated using Eq. (3).

$$\rho_{exp} = \rho_1 * R_1 + \rho_2 * R_2 + \rho_3 * R_3 + \rho_4 * R_4 \qquad (3)$$

where ρ are HPMC, PVP, SiO_2 and APIs density. The density of HPMC, PVP, SiO_2, TXA and PAC are 1.39, 1.20, 2.65, 1.10 and 1.26 g/cm^3, respectively (47-51). *R* is the weight fractions of HPMC, PVP, SiO_2 and APIs within the SSE 3D printed samples. ρ_{exp} is the density of the printed constructs. The porosity was calculated from the percentage of the experimental solid volume ($\mathrm{V_{exp}}$) of the total volume (V_{total}) of the printed construct using Eqs. (4) and (5). *W*, *L* and *T* are the length, width, and thickness of the 3D constructs which were measured at the outermost edges using a vernier calliper.

147 $$V_{total} = W * L * T \quad (4)$$

148 $$Porosity = (1 - \frac{V_{exp}}{V_{total}}) \quad (5)$$

149 The surface morphology of the printed samples was evaluated using scanning electron
150 microscopy (SEM) technique with a Zeiss Gemini 300 (Carl Zeiss AG, Oberkochen,
151 Germany). The samples were sputter-coated with gold prior to scanning. The images
152 were taken at magnifications from 25 to 200 × with an acceleration voltage of 10 kV.

153 **2.7 Physicochemical properties characterisation**

154 A Fourier transform infrared (FTIR) spectrophotometer (VERTEX 70, Bruker Optics,
155 Ettlingen, Germany), equipped with a Golden Gate, Attenuated Total Reflectance
156 (ATR) accessory (Specac Ltd., Orpington, United Kingdom) fitted with a diamond
157 internal reflection element, was used to examine the raw materials, physical mixtures
158 and printed tablets. The spectra were collected over a wavenumber range of 600–4500
159 cm^{-1} with a resolution of 2 cm^{-1} at ambient temperature. As the SSE 3D printed samples
160 were dried at ambient temperature (21 ^{o}C) for 72 h, thermogravimetric analysis (TGA)
161 was conducted using TGA 5500 discovery series (TA Instruments, Newcastle, USA) to
162 identify the moisture content of the dried 3D printed samples. 5–7 mg of sample was
163 loaded into the instrument and subjected to a temperature program of 10 °C/min from
164 25 °C to 700 °C under a nitrogen atmosphere (20 mL/min). Trios (TA Instruments,
165 Newcastle, USA) software was used to analyse the acquired results. All measurements
166 were performed in triplicate on three different tablets.

167 **2.8 Mechanical strength analysis**

168 To evaluate the mechanical strength of the prints, puncture tests were performed on the
169 printed tablets with a TA-XT Plus Texture analyser (Stable Micro Systems), using a

spherical probe (diameter 5 mm). The puncture tests were performed on the centre of the fully dried 3D printed samples (20 × 20 × 3 mm cuboid). Force and displacement data were recorded using Texture Expert from Stable Micro Systems Ltd. software. The speed of the probe was set at 1.0 mm/s during compression. Triplicate measurements on three different tablets were performed.

2.9 *In vitro* drug release study

The *in vitro* drug release behaviours of the drug-loaded constructs were tested in 25 mL of pH 7.4 phosphate-buffered saline (PBS) with 100 rpm agitation at 37 °C in a shaking incubator (IKA, Staufen, Germany). A sink condition was maintained throughout the drug release period. Three millilitres samples were extracted and replenished with an equal volume of fresh medium at predetermined time intervals. Salicylaldehyde (SA) was used as the reagent for the UV spectrophotometry detection of TXA (52). One millilitre of TXA drug solution was added to 1 mL of 1% w/v SA solution. The complete reaction was attained after 12 hours. The UV detection was carried out at 422 nm for TXA and 243 nm for PAC. TXA and PAC samples were placed in a 96-well quartz microplate for UV detection using a CLARIO star microplate reader (BMG Labtech, Ortenberg, Germany). The drug release experiments were performed in triplicate for each construct design.

2.10 Statistical analysis

Numerical data were expressed as the mean ± standard deviation and analysed via Student's t-test to determine the differences among the groups. Statistical significance is indicated when $p \leq 0.05$, while no significance when $p > 0.05$.

3 Results and discussion

3.1 Ink development

3.1.1 Effect of additive and API

The visual inspection of the initial physical appearance of the inks (formulas shown in **Table 1**) after manually stirring for 5 minutes at ambient temperature (21 °C) is presented in the Supplementary Material (**Figure S1a-d**). HPMC at 15 and 30 % w/w did not mix well in water to form a homogenous ink. 20% w/w PVP in water forms an ink solution with low viscosity. An addition of 20% w/w PVP to 15% w/w HPMC transformed the ink into a viscous and homogeneous paste which is ideal for SSE 3D printing.

The effect of the incorporation of API on the inks was studied using TXA and PAC. TXA is a low molecular weight (157.21 g/mol) zwitterionic compound with an aqueous solubility of 167 mg/mL (53) while PAC has an aqueous solubility of 14 mg/mL (54). Owing to the limit of aqueous solubility, only 5% and 15% w/w TXA were fully dissolved in the water, whereas 5% w/w PAC and 30% w/w TXA formed a suspension and crystalline PAC and TXA can be seen by PLM. PAC particulates in the 5% w/w PAC suspension remained observed upon the addition of 15% w/w HPMC dry powders. However, the amount of PAC particulates decreased after the addition of 20% PVP as evident in **Figure 2a-b**. On the other hand, an addition of 15% w/w HPMC and 20% w/w PVP dry powders to the TXA solutions (5 and 15% w/w) and TXA suspension (30% w/w) revealed particulates birefringence in all PLM captures (**Figure 2c-f**). The PLM images of HPMC+PVP with 5% w/w TXA and the blank were noted as extremely similar, as shown in **Figure 2c-d,** proving that some particulates may be the presence of undissolved polymers. No birefringence associated with crystalline TXA particles

was observed, indicating a full dissolution of 5% w/w TXA in HPMC+PVP ink. Unexpectedly, the addition of HPMC and PVP to 15% w/w TXA solution resulted in the recrystallisation of TXA particles, where birefringence of TXA was observed as shown in **Figure 2e**. This observation shows the addition of HPMC and PVP has reduced the aqueous solubility of the TXA drug. As TXA content increased, more crystalline TXA was observed in the PLM images of HPMC+PVP+30TXA ink (**Figure 2f**).

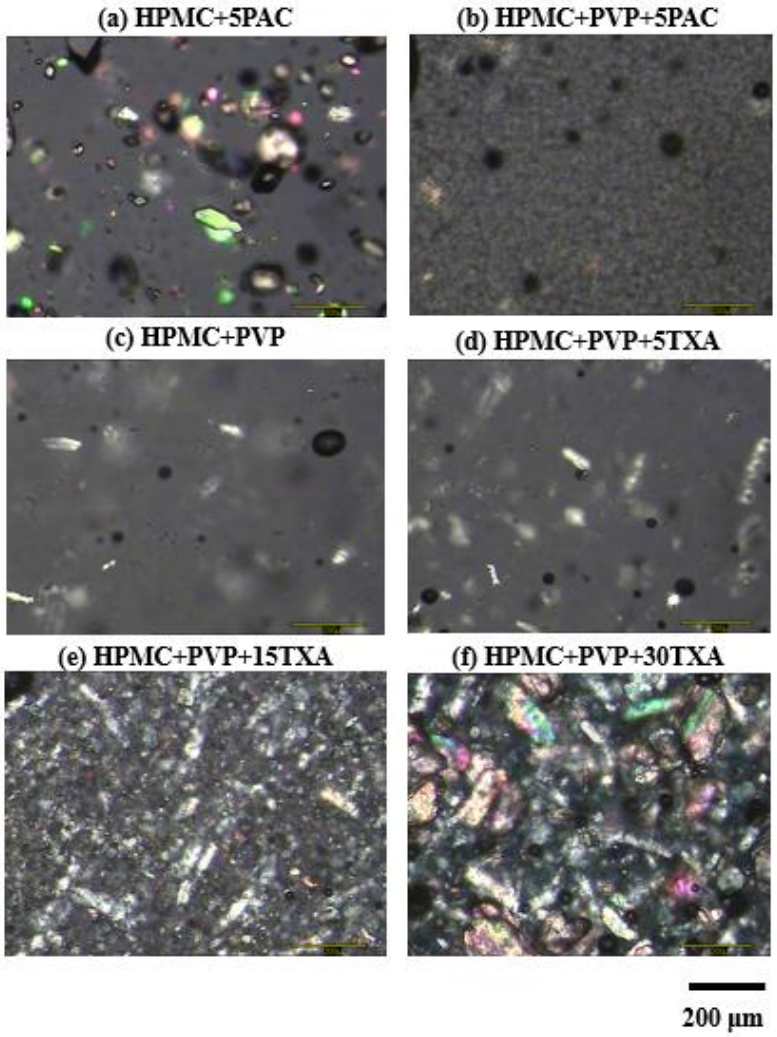

Figure 2. The polarized light microscopy images of the inks with (a) HPMC+5PAC, (b) HPMC+PVP+5PAC, (c) HPMC+PVP, (d) HPMC+PVP+5TXA, (e) HPMC+PVP+15TXA and (f) HPMC+PVP+30TXA.

The rheological properties of all formulated inks were evaluated at steady-state shear viscosity measurements. PVP solution behaves as a Newtonian fluid and shows the lowest viscosity that does not change with shear rate increment (**Figure 3a**). In contrast, HPMC-based inks exhibited non-Newtonian fluid shear thinning behaviour (i.e., the viscosity decreases when the shear rate increases). The low-shear viscosities of inks increased with increasing HPMC concentrations. The addition of PVP to 15HPMC ink did not change the shear-thinning behaviour of the ink. Interestingly, the addition of 20PVP to 15HPMC showed a significant decrease ($p \leq 0.05$) in the low-shear viscosity of the ink (HPMC+PVP) as compared to 30HPMC despite containing a higher percentage weight of solute. This could be due to a possible plasticizing effect by PVP due to hydrogen bond formation (55). Additional PVP also significantly decreases ($p \leq 0.05$) the low-shear viscosity of both PAC and TXA-loaded HPMC-based inks, as shown in **Figure 3b-c**. On the other hand, SiO_2 significantly increased ($p \leq 0.05$) the low-shear viscosity of both PAC and TXA-loaded HPMC+PVP-based inks. Suspension of silica particles in polymer solutions is thixotropic, displaying a gradual increase in their low-shear viscosity. This has been attributed to the formation of a network between polymer chains and the contiguous silica particles (56).

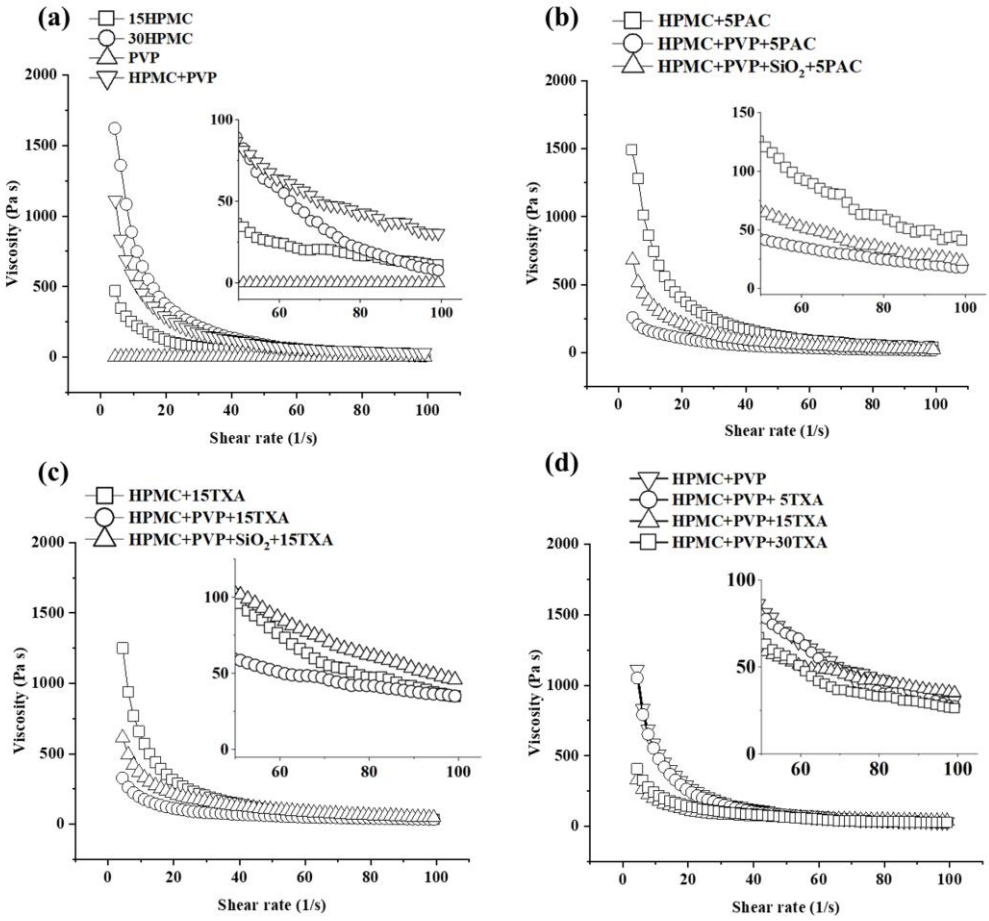

245

246 **Figure 3**. Viscosity shear rate flow curves of the inks. The influences of (a) additive, (b) incorporation
247 of PAC and (c) TXA, and (d) TXA concentration on the ink viscosities. (Detailed ink formulation
248 compositions are presented in **Table 1**.)

249 The influence of TXA concentration on the rheological properties of the inks is shown
250 in **Figure 3d**. The addition of 5% w/w TXA showed no effect on the low-shear
251 viscosity of HPMC+PVP ink. A decrease in low-shear viscosity of inks was noted
252 when TXA concentration increased from 5% to 15% w/w, but no difference was
253 observed from 15% to 30% w/w TXA. This is because TXA has fully dissolved in
254 HPMC+PVP ink at 5% w/w, as described in the PLM images in **Figure 2c-d** but not at
255 15% and 30% w/w.

256

Correlation of ink properties and printed shape fidelity

As ink contains a large amount of solvent (water for this study), solvent evaporation during drying often leads to the shrinkage of the 3D printed constructs and subsequently poor shape fidelity. **Figure 4** shows the physical appearances of 3D printed tablets of HPMC+PVP+15TXA (15% w/w drug loading) and HPMC+PVP+5PAC (5% w/w drug loading) immediately upon complete deposition of all designed layers and 12 hours post-drying at ambient temperature. A thermogravimetric analysis (TGA) on dried HPMC+PVP+15TXA and HPMC+PVP+5PAC samples showed a loss of weight up to 100 ^{o}C (i.e., water content evaporation) by 1.45±0.10% and 0.94±0.31% respectively as presented in the Supplementary Material (Figure S2).

As shown in **Figure 4a**, a great shrinkage in the thickness of all 3D printed tablets was identified. This shrinkage is due to the water loss of SSE 3D printed tablets during the drying process. Pore area changes (defined as the empty void between filaments, as shown in **Figure 4b**) of the top layer of the prints were monitored for 12 hours during drying.

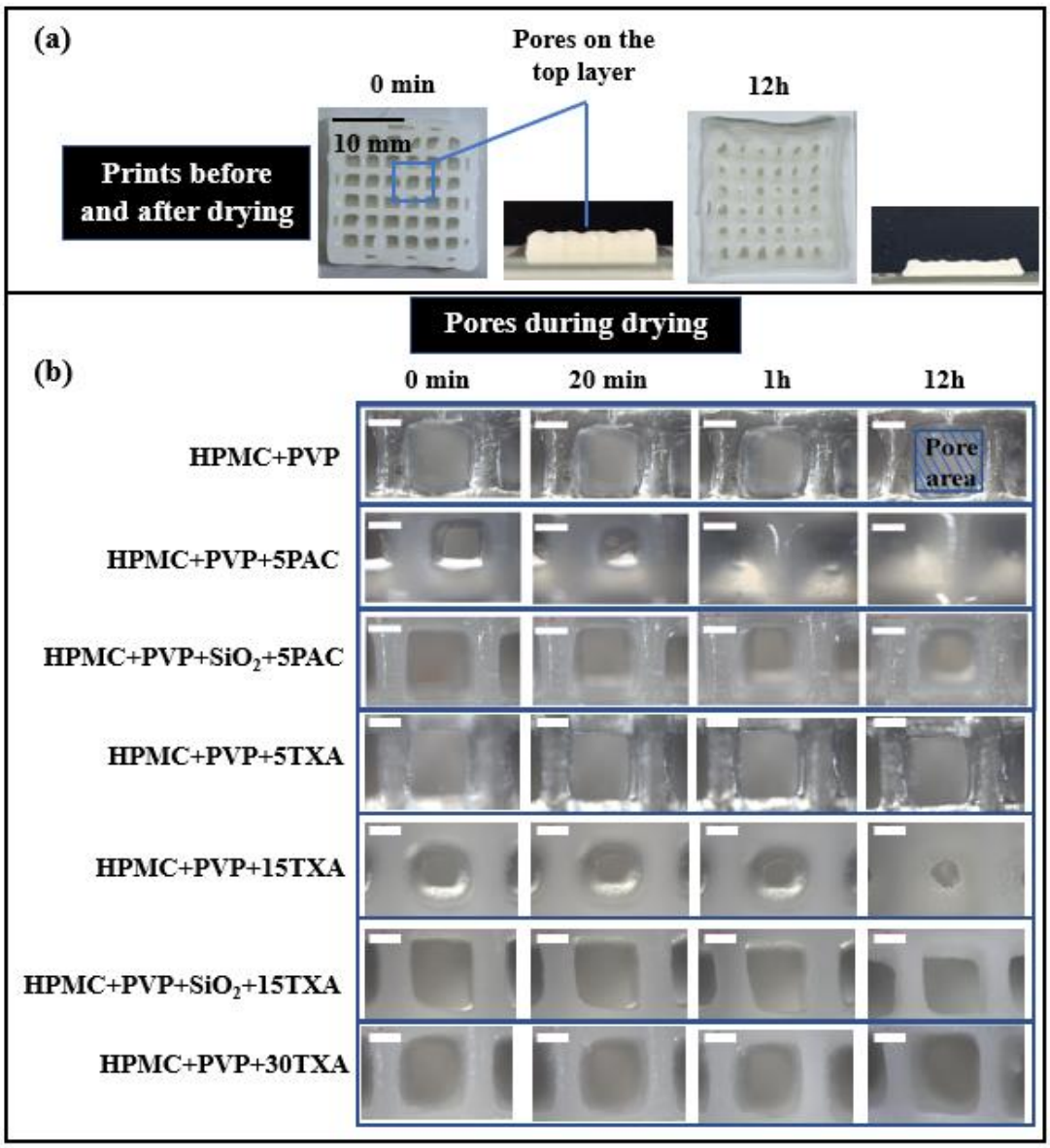

Figure 4. (a) 3D printed HPMC+PVP+15TXA tablet immediately after printing (0 min) and 12 h post-drying at ambient temperature (21 °C); (b) The top pore area changes were observed at the time intervals (0 min, 20 min, 1h and 12 h) for HPMC+PVP, HPMC+PVP+5PAC, HPMC+PVP+SiO_2+5PAC, HPMC+PVP+5TXA, and HPMC+PVP+15TXA, HPMC+PVP+SiO_2+15TXA, and HPMC+PVP+30TXA (scale bar in (b) represents 900 μm).

To evaluate the effect of API concentration on shape fidelity, a range of inks with different TXA concentrations (5, 15 and 30% w/w) were studied. As shown in **Figure 4**, the shape fidelities of drug-loaded prints were compared to the blank ink base by

utilising the pore structures as the key indicator. TXA was fully dissolved in ink when 5% w/w was loaded but partially dissolved at 15% and 30% w/w. This indicates that HPMC+PVP and HPMC+PVP+5TXA inks initially had no solid contents. In contrast, HPMC+PVP+15TXA ink contains an amount of solid crystalline drug particles and worse in HPMC+PVP+30TXA.

As depicted in **Figure 4b**, HPMC+PVP, HPMC+PVP+5TXA and HPMC+PVP+30TXA prints showed small change in pore areas during drying, whereas HPMC+PVP+15TXA print showed nearly 50.5±1.1% pore area under-sizing during the 12 hours drying. This seems to contradict the observation in PAC where solid content increment would improve shape fidelity. The viscosity data shown in **Figure 3d** revealed nearly identical viscosities of HPMC+PVP and HPMC+PVP+5TXA inks, which are significantly higher than the viscosities of the inks with 15% and 30% w/w drug loading. It is clear at this point that the fully dissolved 5% w/w TXA showed no impact on the viscosity of the HPMC-PVP solution. This may explain the good shape fidelities of the HPMC+PVP and HPMC+PVP+5TXA inks after printing and drying.

In 30% w/w TXA drug-loaded ink, consistent nozzle blockage was observed during 3D printing which hurdle the replication of sample printing. This could be reasoned due to the accumulation of undissolved TXA with unknown particle size and subsequently lead to nozzle blockage (diameter of 413 μm) during the extrusion process of 3D printing. Therefore, only HPMC+PVP+5TXA and HPMC+PVP+15TXA 3D printed tablets were subjected to further investigate the effect of drug concentration on drug release. As the concentration of TXA increased, it was noted that the low-shear viscosity of HPMC+PVP+15TXA and HPMC+PVP+30TXA inks significantly

reduced ($p \leq 0.05$). Based on the observation of the rheological behaviour of 5% w/w drug-loaded ink against the blank, dissolved TXA within the ink did not affect the low-shear viscosity ($p \geq 0.05$). This indicates the undissolved TXA particles have led to a viscosity reduction, particularly when high drug concentrations were loaded. For HPMC+PVP+30TXA ink, the high amount of particulate contents could pack together during drying and subsequently inhibit the ink flow which resulted in the observed lack of pore area changes (26).

The corresponding pore area under-sizing percentage with the time is shown in **Figure 5**. The pores of HPMC+PVP+5PAC prints were completely closed and disappeared after 12 hours of drying. HPMC+PVP+15TXA showed a significant under-sizing in pore areas ($p \leq 0.05$), but not a complete pore closure. The pore area of HPMC+PVP+15TXA decreased by 50.5±1.1% after 12 hours. The addition of SiO_2 (which is an insoluble and structuring additive for both ink formulations) significantly improved ($p \leq 0.05$) the shape fidelities of the prints after drying and avoided pore closures. HPMC+PVP+ SiO_2+15TXA ink maintained the shape fidelity much better than HPMC+PVP+15TXA during drying. This could be attributed to the high solid contents in the HPMC+PVP +SiO_2+15TXA ink formula.

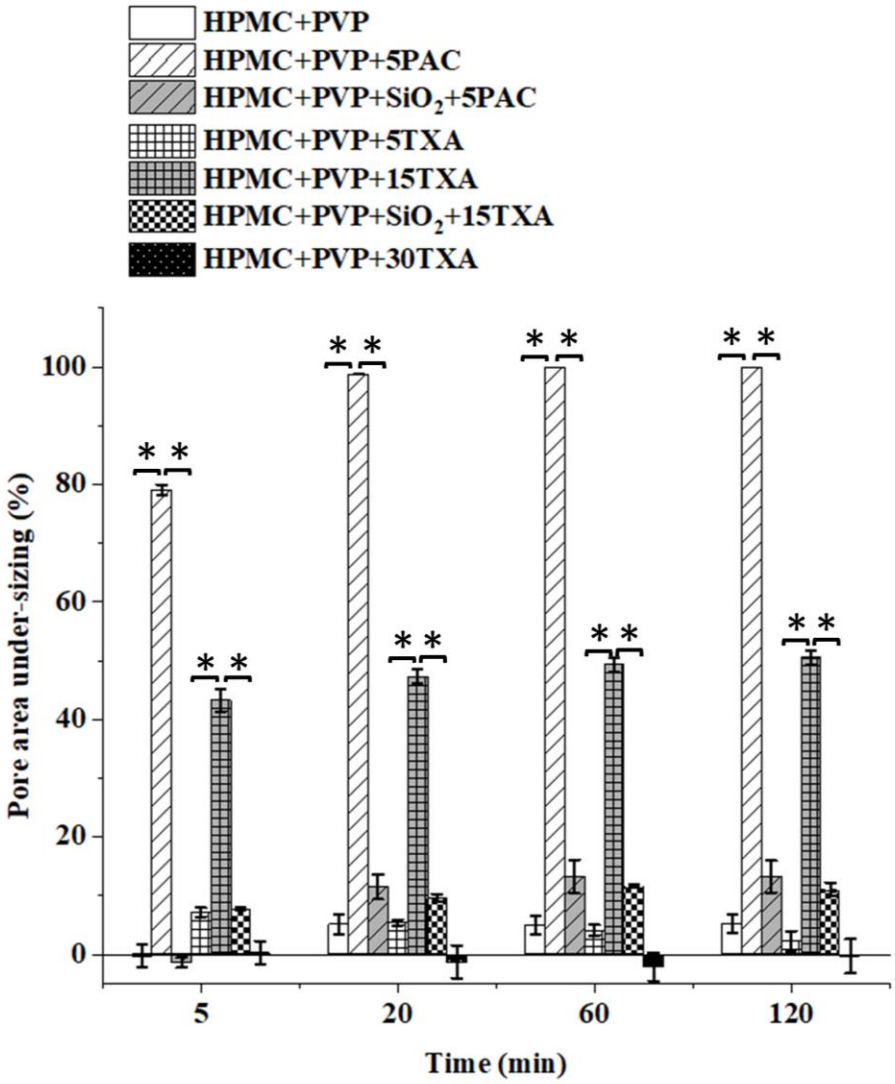

323

324 **Figure 5**. Pore area under-sizing (%) over time for the 3D printed tablets of HPMC+PVP,

325 HPMC+PVP+5PAC, HPMC+PVP+SiO_2+5PAC, HPMC+PVP+5TXA, and HPMC+PVP+15TXA,

326 HPMC+PVP+SiO_2+15TXA and HPMC+PVP+30TXA (* indicating $p \leq 0.05$).

327 The physical appearances and SEM images of post-drying 3D printed HPMC+PVP inks

328 loaded with TXA and PAC are shown in **Figure 6**. A greater pore area reduction

329 occurred in the tablets printed using inks without SiO_2, and the pores were completely

330 sealed in the samples printed using the PAC-loaded ink. This is likely to be due to the

331 decrease in the low-shear viscosity of ink (as shown in **Figure 3d**). The addition of

332 SiO_2 to the inks increased the solid content of the inks. This led to a significant increase

in the low-shear viscosities of inks ($p \leq 0.05$) with both drugs in comparison to the inks without SiO_2. The higher solid content translated into a lower solvent content and in turn shortened the drying. The higher viscosity led to weaker spreading and flow of the ink during drying. The combination of both high solid content and high viscosity led to the improvement in shape fidelity.

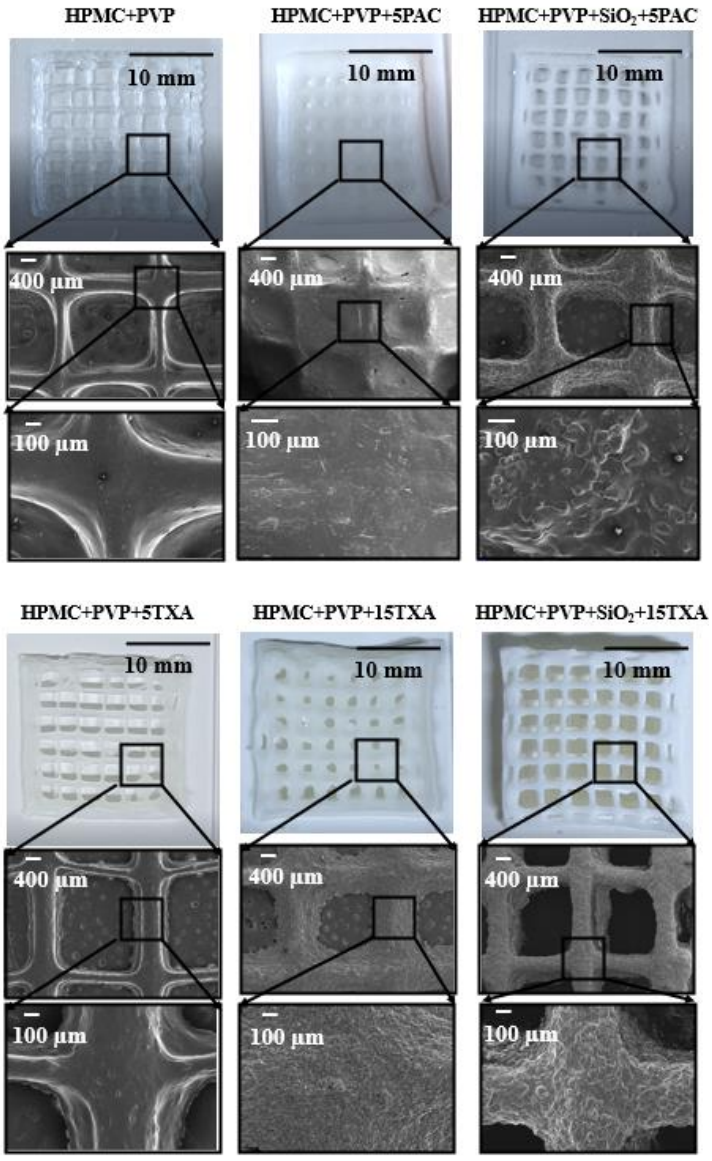

Figure 6. Physical appearances and SEM images of dried 3D printed tablets of HPMC+PVP, HPMC+PVP+5PAC, HPMC+PVP+SiO_2+5PAC, HPMC+PVP+5TXA, and HPMC+PVP+15TXA, HPMC+PVP+SiO_2+15TXA.

342 ATR-FTIR was carried out to investigate any possible molecular interactions between
343 the polymer, additive, and API. The ATR-FTIR spectra of HPMC, PVP, PAC, TXA,
344 physical mixture and dried SSE 3D printed tablets are shown in **Figure 7a-b**. The
345 spectrum of HPMC shows an absorption band at 3445 cm^{-1} assigned to the stretching
346 frequency of the hydroxyl (-OH) group. Other stretching vibration bands related to C-
347 H and C-O were observed at 2929 cm^{-1} and 1056 cm^{-1}, respectively. The peaks of pure
348 HPMC were similar to the literature (57). The FTIR spectrum of PVP displays a peak
349 at 3424 cm^{-1}, assigned to O-H stretching. The peaks at 2950 cm^{-1} and 1652 cm^{-1} were
350 assigned to asymmetric stretching of CH_2 and stretching of C-O, respectively (58). As
351 seen in **Figure 7a**, the spectrum of PAC shows a characteristic vibrational peak for NH
352 stretching at 3326 cm^{-1} due to the presence of crystalline material (59, 60).
353

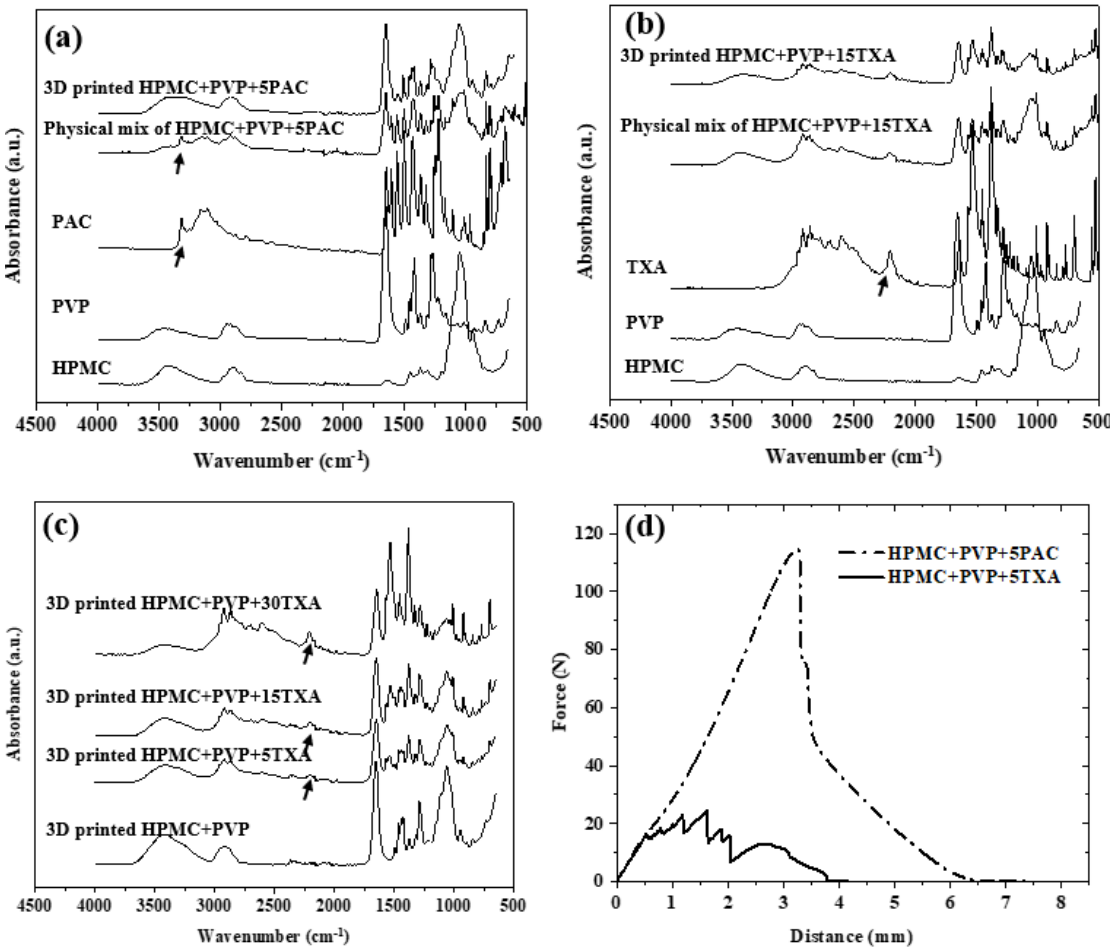

Figure 7. FTIR results of PAC-loaded HPMC+PVP 3D printed tablet (a), TXA-loaded HPMC+PVP 3D printed tablet (b), HPMC+PVP+TXA tablets with various TXA concentrations (c), and the mechanical properties of HPMC+PVP+5PAC and HPMC+PVP+5TXA tablets obtained from puncture tests. The curves displayed for the puncture test were plotted with average values from three replicates.

In contrast to the pure PAC and physical mixture HPMC+PVP+PAC, the sharp peak of N-H stretching at 3326 cm^{-1} (as the arrow indicated in **Figure 7a**) has disappeared in 3D printed HPMC+PVP+PAC. This is likely due to PVP interacting with PAC *via* hydrogen bonding and potentially reducing the crystallinity of PAC (**Figure 1 b, c**). This is also supported by the preliminary DSC data as shown in Figure S3. The thermogram depicted a melting peak of PAC (159.50±2.15°C) in the physical mixture HPMC+PVP+PAC, but an absence in the dried SSE printed HPMC+PVP+PAC.

As seen in **Figure 7b**, the spectrum of TXA shows a strong cluster of peaks in the region 3000 to 2500 cm^{-1}, representing both NH^{3+} and CH vibrational modes of TXA. (22). There was no significant shift or new peak formation/disappearance in comparison to the physical mixture HPMC+PVP+TXA and 3D printed HPMC+PVP+TXA. FTIR spectra of HPMC+PVP+TXA tablets with various TXA concentrations as shown in **Figure 7c** reported as the concentration increased from 5% to 30% w/w, the intensity of the characteristic peak in 2250 cm^{-1} increased as expected.

3.1.2 Effect of structural design

Table 3 shows the dimensions of the 3D printed tablets resulting from the influence of additive, drug concentration, layer quantity (4 or 14 layers), and infill percentage (25 or 50% infill). There was no significant difference (p = 0.51) in terms of outer dimensional measures (width and length) of the printed tablets HPMC+15TXA, HPMC+PVP+15TXA and HPMC+PVP+SiO_2+15TXA. However, a significant difference in tablet thickness and weight was observed. This is due to the substantial increase in solute concentrations (**Table 1**). As the TXA concentration increased from 0% to 15% w/w, the tablet thickness and weight of HPMC+PVP, HPMC+PVP+5TXA and HPMC+PVP+15TXA increased significantly (p< 0.05).

As expected, the layer number affects tablet thickness and weight. For instance, the tablet thickness and weight for HPMC+PVP+5TXA_14 layer are roughly 3 times of HPMC+PVP+5TXA_4 layer. No significant difference in width, length and thickness among the 3D printed tablets with different drug loadings and infills (HPMC+PVP+5TXA_25%infill, HPMC+PVP+15TXA_25%infill,

389 HPMC+PVP+5TXA_50%infill and HPMC+PVP+15TXA_50%infill) were noted, but

390 a significant difference regarding the tablet weight were expected.

391 **Table 3**. Dimension, porosity, and weight of the SSE 3D printed tablet.

	Width (mm)	**Length (mm)**	**Thickness (mm)**	**Pore area (mm^2)**	**Tablet weight (mg)**	**Porosity (%)**
Influence of additive & API						
HPMC+PVP	19.9±0.1	19.9±0.1	1.3±0.1	3.8±0.1	203.8±21.8	69.8±1.9
HPMC+PVP+5TXA	19.6±0.4	19.4±0.4	1.8±0.1	3.9±0.1	252.7±16.3	72.0±1.0
HPMC+15TXA	18.5±0.0	18.5±0.1	1.8±0.2	3.9±0.1	144.2±4.2	82.9±1.3
HPMC+PVP+15TXA	18.9±0.1	18.7±0.2	20.0±0.0	2.0±0.0	286.2±1.3	67.7±1.0
HPMC+PVP+SiO2+15TXA	17.7±0.4	17.9±0.3	2.4±0.1	3.6±0.1	312.7±4.9	69.1±2.6
HPMC+PAC	19.9±0.2	20.0±0.1	0.6±0.0	1.8±0.2	73.7±11.1	76.4±2.3
HPMC+PVP+5PAC	19.6±0.4	19.8±0.2	0.9±0.0	0*	223.4±3.3	47.6±2.1
HPMC+PVP+SiO2+5PAC	19.8±0.3	19.8±0.3	1.5±0.0	3.5±0.1	231.4±6.1	70.3±0.2
Influence of structural design						
HPMC+PVP+5TXA_4layer	19.7±0.1	19.6±0.9	0.6±0.1	3.9±0.1	84.6±11.3	70.6±0.7
HPMC+PVP+15TXA_4layer	19.7±0.1	19.6±0.1	0.5±0.0	2.5±0.8	81.2±0.6	67.9±0.8
HPMC+PVP+5TXA_14layer	19.6±0.4	19.4±0.4	1.8±0.1	3.9±0.1	252.7±16.3	72.0±1.0
HPMC+PVP+15TXA_14layer	18.9±0.1	18.7±0.2	2.0±0.0	2.0±0.0	286.2±1.3	67.7±1.0
HPMC+PVP+5TXA_25%infill	19.6±0.4	19.4±0.4	1.8±0.1	3.9±0.1	252.7±16.3	72.0±1.0
HPMC+PVP+15TXA_25%infill	18.9±0.1	18.7±0.2	2.0±0.0	2.0±0.0	286.2±1.3	67.7±1.0
HPMC+PVP+5TXA_50%infill	18.3±0.1	18.6±0.0	1.9±0.1	0.4±0.1	357.7±14.8	57.1 ±1.0
HPMC+PVP+15TXA_50%infill	18.7±0.2	18.5±0.0	2.1±0.1	0*	463.3±1.8	48.5±2.8

392 *The pores were fully merged during drying.

3.2 Drug release of 3D printed tablet

3.2.1 Effect of additive and API

The influence of the additive on the drug release of PAC-loaded tablets was investigated (as shown in **Figure 8a**). The addition of PVP without SiO_2 showed a significant decrease in the drug release rate of PAC ($p < 0.05$). This may be due to the porosity of HPMC+PVP+PAC (≈48%) being significantly lower than tablets without PVP or with both PVP and SiO_2 (≈70-76%). The addition of SiO_2 to HPMC+PVP+PAC ink significantly increased the drug release rate ($p < 0.05$) and reached a similar rate as HPMC+PAC without PVP. The increased drug release of HPMC+PVP+SiO_2+PAC in comparison to HPMC+PVP+PAC is likely to be due to SiO_2 acting as a disintegrant and speeding up the dissolution process, as discussed in other studies (61, 62).

The influence of the additive on the *in vitro* drug release of the TXA-loaded 3D printed tablet is shown in **Figure 8b**. The addition of PVP and SiO_2 showed no significant impacts on the drug release rate of HPMC+15TXA, HPMC+PVP+15TXA and HPMC+PVP+SiO_2+15TXA tablets. As shown in **Table 3**, the pore area of HPMC+15TXA, HPMC+PVP+15TXA and HPMC+PVP+SiO_2+15TXA are 3.9±0.1, 2.0±0.0 and 3.6±0.1 mm^2. Despite having the smallest pore area (67.7±1.0%) within the dried prints, the porosity of HPMC+PVP+15TXA is not significantly lower than HPMC+PVP+SiO_2+15TXA (69.1±2.6%). Thus, the drug release of HPMC+PVP+15TXA was not significantly slower than the other two (i.e., HPMC+15TXA and HPMC+PVP+SiO_2+15TXA).

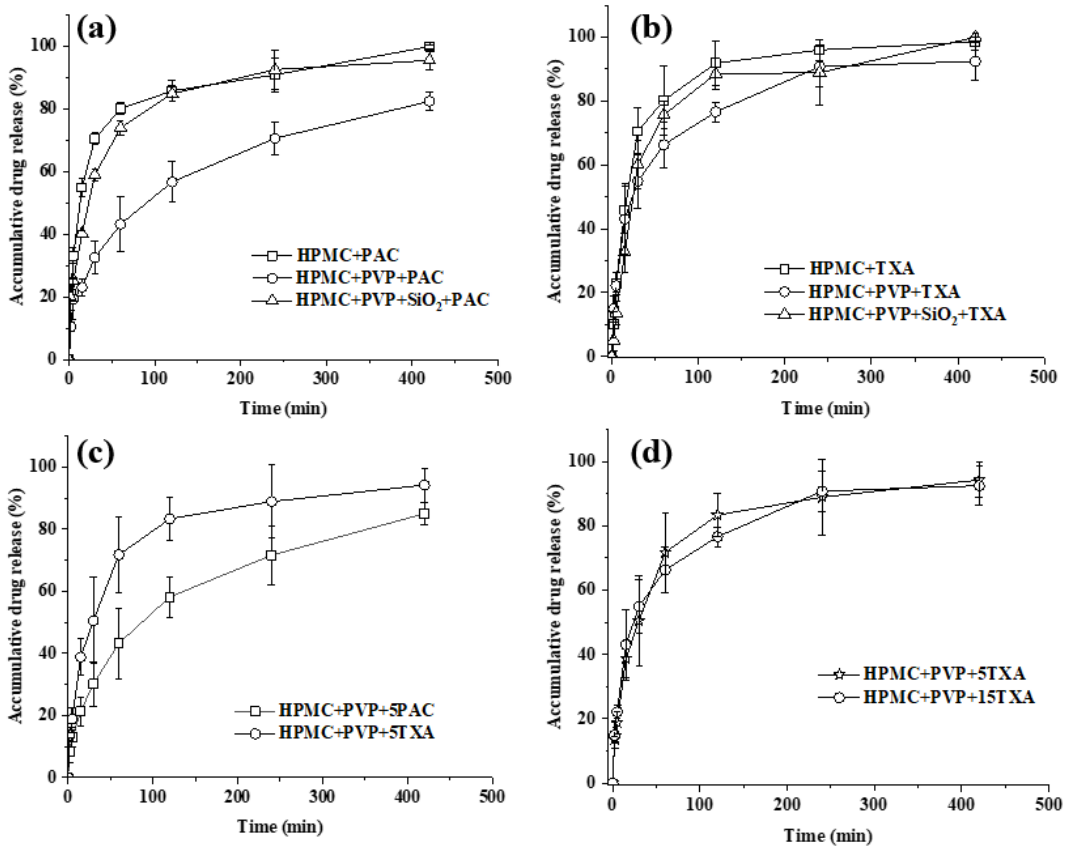

Figure 7. *In vitro* drug release data of SSE 3D printed tablets of (a) PAC-loaded tablets, (b) TXA-loaded tablets, (c) the influence of API type, and (d) the influence of API concentration.

The influence of API type on the drug release rate is shown in **Figure 8c**. The drug release of PAC-loaded tablets was significantly lower than the one loaded with TXA, despite both having the same (5% w/w) drug loading in the ink. This is possibly due to the porosity of HPMC+PVP+5TXA being significantly higher than HPMC+PVP+5PAC, which are 72.0±1.0% and 47.6±2.1%, respectively. Another possible reason is TXA-based tablets can easily disintegrate during drug dissolution, which was proved by the puncture mechanical test where TXA tablets require much less force to puncture than PAC tablets. The influence of TXA concentration on drug release has been investigated and illustrated in **Figure 8d**. There was no significant difference between 5% and 15% w/w TXA drug loadings. Although the pore area of

HPMC+PVP+5TXA is higher than HPMC+PVP+15TXA, yet, no significant difference ($p > 0.05$) was identified. This could be due to the limitation of measuring pore area by 2D-microscopy images, but porosity existed in three dimensions. Due to the advantage of 3D printing technique, it is possible to have voids in between the 3D printed HPMC+PVP+15TXA_14layer despite a fully merged (pore area = 0 mm^2) of the 2D pore area was observed.

3.2.2 Effect of structural design

The influence of the number of layers on the drug release rates of the tablets is shown in **Figure 9a-b**. As TXA is a highly water-soluble drug and the drug was fully dissolved in the printed tablets at a drug loading of 5% w/w, theoretically, the release rate limiting factor would be the dissolution of the polymeric matrices. 14- and 4-layer prints have a 3-fold thickness difference, which should be translated into a difference in dissolution rate. However, there was no difference in the drug release rate of the 14- and 4-layers tablets with 5% w/w TXA (**Figure 9a**). This is possibly due to the insignificant difference in pore area and porosity between 14- and 4-layers prints and the ease of tablet disintegration. Both tablets were similar in terms of pore area (3.9±0.1 mm^2) and porosity (71.5±1.6%).

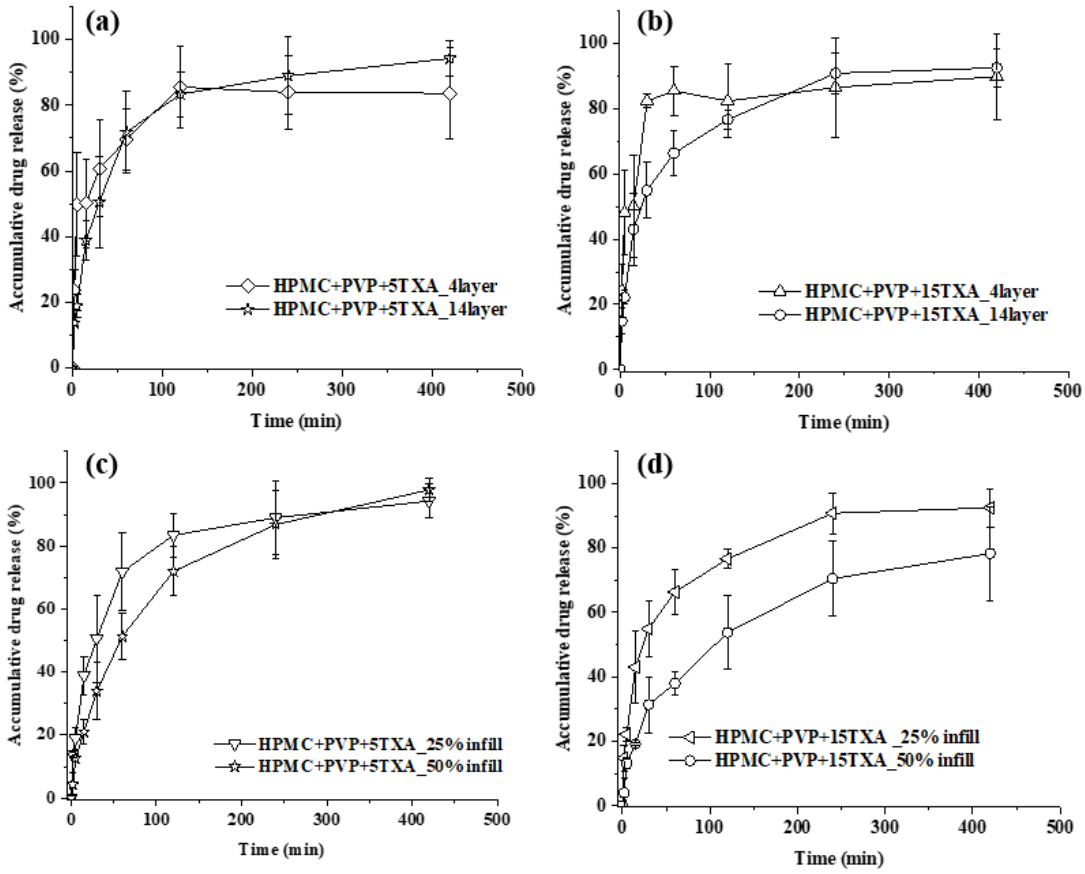

Figure 9. *In vitro* drug release profiles of (a) 5%TXA-loaded tablets and (b) 15%TXA-loaded tablets affected by layer number factor, and (c) 5%TXA-loaded tablets and (d) 15%TXA-loaded tablets affected by infill percentage.

As shown in **Figure 9b**, when the loaded drug was increased to 15% w/w, where a significant amount of undissolved drug was present in the prints, the 4-layers drug release rate was significantly higher than the 14-layers between 60-120 minutes. This is possibly due to the higher pore area of 4-layers (2.0±0.0 mm^2) compared to 14-layer (2.5±0.8 mm^2).

The infill showed no effect on the drug release rate of the prints loaded with 5% w/w TXA (**Figure 9c**) but significantly affected the prints loaded with 15% w/w TXA (**Figure 9d**). This could be due to the significantly lower viscosity of 15% w/w TXA

ink than the 5% w/w TXA ink and that resulted in an almost entirely merged of pores within the 3D printed HPMC+PVP+15TXA tablets with 50% infill. The porosity of HPMC+PVP+15TXA_50%infill and HPMC+PVP+15TXA_25%infill were reported at 48.5±2.8% and 57.1±1.0%, respectively. In summary, the drug release rates of all TXA drug-loaded 3D printed tablets were lower than the pure TXA powder.

4 Conclusion

This study developed an understanding of the influence of additive and API on the prints of SSE 3D printing and their drug release performance. HPMC and binary polymeric system HPMC-PVP-based semisolid inks have been developed for SSE 3D tablet printing. The influence of additive (i.e., SiO_2) and API (i.e., PAC and TXA) on ink rheology behaviour, 3D printing shape fidelity and drug release performance have been investigated and demonstrated. It was shown that the use of additive, API candidate selection and concentration could significantly affect the ink rheology behaviour and further change the shape fidelity of SSE 3D printed tablets. A clear relationship between the low shear viscosity of the semisolid ink and their printability was observed. The API (i.e., PAC and TXA) loaded inks for 3D printing showed more significant pore merging issues than the blank HPMC-PVP based inks. The addition of SiO_2 proved to relieve the pore merging issue. This could be observed from the pore area improvement of HPMC+PVP+SiO_2+5PAC prints at 3.5±0.1 mm^2 compared to the completely closed (0 mm^2) HPMC+PVP+5PAC prints after 12 hours of drying. HPMC+PVP+15TXA formulation showed a significant under-sizing in pore areas ($p \leq 0.05$) at 50.5±1.1% after 12 hours of drying. The addition of SiO_2 significantly improved the pore area of the prints to 41.0±2.2%. The drug release study showed the

drug release rate was affected by the selection of polymeric system and API. PVP showed a significant delay ($p \leq 0.05$) in the drug release of PAC-loaded tablets, possibly due to the poor porosity. Besides, it was noted that the structural properties of 3D printed tablets also affected drug release. Investigation into the layer numbers and infill density showed the layer number had little effect but the infill percentage of TXA tablets significantly influenced drug release, probably due to the effects of pore merging. The insights reported in this study could serve as practical guidance for ink development in fabricating a controlled performance SSE 3D printed porous formulation for personalised pharmaceuticals.

Acknowledgement

This research was funded by the Redistributed Manufacturing in Healthcare Network (RiHN). RiHN was awarded a grant from the UK Engineering and Physical Sciences Research Council (EPSRC) (Ref. EP/T014970/1). The authors thank Thomas McDonagh for his help with the mechanical testing.

References

1. Hsiao W-K, Lorber B, Reitsamer H, Khinast J. 3D printing of oral drugs: a new reality or hype? Expert Opinion on Drug Delivery. 2018;15(1):1-4.
2. Wening K, Breitkreutz J. Oral drug delivery in personalized medicine: unmet needs and novel approaches. International Journal of Pharmaceutics. 2011;404(1-2):1-9.
3. Martinez PR, Goyanes A, Basit AW, Gaisford S. Fabrication of drug-loaded hydrogels with stereolithographic 3D printing. International journal of pharmaceutics. 2017;532(1):313-7.
4. Asikainen S, van Bochove B, Seppälä JV. Drug-releasing biopolymeric structures manufactured via stereolithography. Biomedical Physics & Engineering Express. 2019;5(2):025008.
5. Fina F, Goyanes A, Madla CM, Awad A, Trenfield SJ, Kuek JM, et al. 3D printing of drug-loaded gyroid lattices using selective laser sintering. International Journal of Pharmaceutics. 2018;547(1-2):44-52.
6. Wickström H, Hilgert E, Nyman JO, Desai D, Şen Karaman D, De Beer T, et al. Inkjet printing of drug-loaded mesoporous silica nanoparticles—A platform for drug development. Molecules. 2017;22(11):2020.
7. Boehm RD, Miller PR, Daniels J, Stafslien S, Narayan RJ. Inkjet printing for pharmaceutical applications. Materials Today. 2014;17(5):247-52.
8. Alhijjaj M, Nasereddin J, Belton P, Qi S. Impact of processing parameters on the quality of pharmaceutical solid dosage forms produced by fused deposition modeling (FDM). Pharmaceutics. 2019;11(12):633.
9. Gültekin HE, Tort S, Acartürk F. An Effective Technology for the Development of Immediate Release Solid Dosage Forms Containing Low-Dose Drug: Fused Deposition Modeling 3D Printing. Pharmaceutical research. 2019;36(9):128.
10. Goyanes A, Martinez PR, Buanz A, Basit AW, Gaisford S. Effect of geometry on drug release from 3D printed tablets. International journal of pharmaceutics. 2015;494(2):657-63.
11. Korte C, Quodbach J. 3D-printed network structures as controlled-release drug delivery systems: dose adjustment, API release analysis and prediction. AAPS PharmSciTech. 2018;19(8):3333-42.
12. Goyanes A, Allahham N, Trenfield SJ, Stoyanov E, Gaisford S, Basit AW. Direct powder extrusion 3D printing: Fabrication of drug products using a novel single-step process. International journal of pharmaceutics. 2019;567:118471.
13. Boniatti J, Januskaite P, Fonseca LBd, Viçosa AL, Amendoeira FC, Tuleu C, et al. Direct powder extrusion 3d printing of praziquantel to overcome neglected disease formulation challenges in paediatric populations. Pharmaceutics. 2021;13(8):1114.
14. Sánchez-Guirales SA, Jurado N, Kara A, Lalatsa A, Serrano DR. Understanding direct powder extrusion for fabrication of 3D printed personalised medicines: A case study for nifedipine minitablets. Pharmaceutics. 2021;13(10):1583.
15. Mcdonagh T, Belton P, Qi S. An investigation into the effects of geometric scaling and pore structure on drug dose and release of 3D printed solid dosage forms. European Journal of Pharmaceutics and Biopharmaceutics. 2022.

16. McDonagh T, Belton P, Qi S. Direct granule feeding of thermal droplet deposition 3D printing of porous pharmaceutical solid dosage forms free of plasticisers. Pharmaceutical Research. 2022;39(3):599-610.
17. Zhang B, Gleadall A, Belton P, Mcdonagh T, Bibb R, Qi S. New insights into the effects of porosity, pore length, pore shape and pore alignment on drug release from extrusionbased additive manufactured pharmaceuticals. Additive Manufacturing. 2021;46:102196.
18. Nasereddin JM, Wellner N, Alhijjaj M, Belton P, Qi S. Development of a simple mechanical screening method for predicting the feedability of a pharmaceutical FDM 3D printing filament. Pharmaceutical research. 2018;35(8):151.
19. Goyanes A, Fina F, Martorana A, Sedough D, Gaisford S, Basit AW. Development of modified release 3D printed tablets (printlets) with pharmaceutical excipients using additive manufacturing. International journal of pharmaceutics. 2017;527(1-2):21-30.
20. Isreb A, Baj K, Wojsz M, Isreb M, Peak M, Alhnan MA. 3D printed oral theophylline doses with innovative 'radiator-like'design: Impact of polyethylene oxide (PEO) molecular weight. International journal of pharmaceutics. 2019;564:98-105.
21. Dumpa N, Butreddy A, Wang H, Komanduri N, Bandari S, Repka MA. 3D printing in personalized drug delivery: An overview of hot-melt extrusion-based fused deposition modeling. International journal of pharmaceutics. 2021;600:120501.
22. Zhang B, Teoh XY, Yan J, Gleadall A, Belton P, Bibb R, et al. Development of combi-pills using the coupling of semi-solid syringe extrusion 3D printing with fused deposition modelling. International Journal of Pharmaceutics. 2022;625:122140.
23. Truby RL, Lewis JA. Printing soft matter in three dimensions. Nature. 2016;540(7633):371-8.
24. Dávila JL, d'Ávila MA. Rheological evaluation of Laponite/alginate inks for 3D extrusion-based printing. The International Journal of Advanced Manufacturing Technology. 2019;101(1-4):675-86.
25. Zhang B, Cristescu R, Chrisey DB, Narayan RJ. Solvent-based Extrusion 3D Printing for the Fabrication of Tissue Engineering Scaffolds. International Journal of Bioprinting. 2020;6(1).
26. Teoh X-Y, Zhang B, Belton P, Chan S-Y, Qi S. The effects of solid particle containing inks on the printing quality of porous pharmaceutical structures fabricated by 3D semi-solid extrusion printing. Pharmaceutical Research. 2022;39(6):1267-79.
27. Seoane-Viaño I, Januskaite P, Alvarez-Lorenzo C, Basit AW, Goyanes A. Semi-solid extrusion 3D printing in drug delivery and biomedicine: Personalised solutions for healthcare challenges. Journal of Controlled Release. 2021;332:367-89.
28. Cheng Y, Qin H, Acevedo NC, Jiang X, Shi X. 3D Printing of Extended-Release Tablets of Theophylline Using Hydroxypropyl Methylcellulose (HPMC) Hydrogels. International Journal of Pharmaceutics. 2020:119983.
29. Compton BG, Lewis JA. 3D ‐ printing of lightweight cellular composites. Advanced materials. 2014;26(34):5930-5.
30. Cui M, Pan H, Fang D, Qiao S, Wang S, Pan W. Fabrication of high drug loading levetiracetam tablets using semi-solid extrusion 3D printing. Journal of Drug Delivery Science and Technology. 2020;57:101683.

31. Khaled SA, Alexander MR, Wildman RD, Wallace MJ, Sharpe S, Yoo J, et al. 3D extrusion printing of high drug loading immediate release paracetamol tablets. International journal of pharmaceutics. 2018;538(1-2):223-30.
32. Khaled SA, Burley JC, Alexander MR, Yang J, Roberts CJ. 3D printing of five-in-one dose combination polypill with defined immediate and sustained release profiles. Journal of controlled release. 2015;217:308-14.
33. Zhang B, Nguyen AK, Narayan RJ, Huang J. Direct ink writing of vancomycin‐loaded polycaprolactone/polyethylene oxide/hydroxyapatite 3D scaffolds. Journal of the American Ceramic Society. 2022;105(3):1821-40.
34. Khaled SA, Burley JC, Alexander MR, Roberts CJ. Desktop 3D printing of controlled release pharmaceutical bilayer tablets. International journal of pharmaceutics. 2014;461(1-2):105-11.
35. Firth J, Basit AW, Gaisford S. The role of semi-solid extrusion printing in clinical practice. 3D printing of pharmaceuticals. 2018:133-51.
36. Sjöholm E, Sandler N. Additive manufacturing of personalized orodispersible warfarin films. International Journal of Pharmaceutics. 2019;564:117-23.
37. Yan T-T, Lv Z-F, Tian P, Lin M-M, Lin W, Huang S-Y, et al. Semi-solid extrusion 3D printing ODFs: an individual drug delivery system for small scale pharmacy. Drug Development and Industrial Pharmacy. 2020;46(4):531-8.
38. Rycerz K, Stepien KA, Czapiewska M, Arafat BT, Habashy R, Isreb A, et al. Embedded 3D printing of novel bespoke soft dosage form concept for pediatrics. Pharmaceutics. 2019;11(12):630.
39. Tagami T, Ito E, Kida R, Hirose K, Noda T, Ozeki T. 3D printing of gummy drug formulations composed of gelatin and an HPMC-based hydrogel for pediatric use. International Journal of Pharmaceutics. 2021;594:120118.
40. Khaled SA, Burley JC, Alexander MR, Yang J, Roberts CJ. 3D printing of tablets containing multiple drugs with defined release profiles. International journal of pharmaceutics. 2015;494(2):643-50.
41. Díaz-Torres E, Rodríguez-Pombo L, Ong JJ, Basit AW, Santoveña-Estévez A, Fariña JB, et al. Integrating pressure sensor control into semi-solid extrusion 3D printing to optimize medicine manufacturing. International Journal of Pharmaceutics: X. 2022;4:100133.
42. Goyanes A, Madla CM, Umerji A, Piñeiro GD, Montero JMG, Diaz MJL, et al. Automated therapy preparation of isoleucine formulations using 3D printing for the treatment of MSUD: First single-centre, prospective, crossover study in patients. International Journal of Pharmaceutics. 2019;567:118497.
43. Vithani K, Goyanes A, Jannin V, Basit AW, Gaisford S, Boyd BJ. An overview of 3D printing technologies for soft materials and potential opportunities for lipid-based drug delivery systems. Pharmaceutical research. 2019;36(1):1-20.
44. Sung K, Nixon PR, Skoug JW, Ju TR, Gao P, Topp E, et al. Effect of formulation variables on drug and polymer release from HPMC-based matrix tablets. International journal of pharmaceutics. 1996;142(1):53-60.
45. Kaneda Y, Tsutsumi Y, Yoshioka Y, Kamada H, Yamamoto Y, Kodaira H, et al. The use of PVP as a polymeric carrier to improve the plasma half-life of drugs. Biomaterials. 2004;25(16):3259-66.

46. Qian KK, Bogner RH. Application of mesoporous silicon dioxide and silicate in oral amorphous drug delivery systems. Journal of pharmaceutical sciences. 2012;101(2):444-63.
47. Friesen DT, Shanker R, Crew M, Smithey DT, Curatolo W, Nightingale J. Hydroxypropyl methylcellulose acetate succinate-based spray-dried dispersions: an overview. Molecular Pharmaceutics. 2008;5(6):1003-19.
48. Pertoft H, Laurent TC, Låås T, Kågedal L. Density gradients prepared from colloidal silica particles coated by polyvinylpyrrolidone (Percoll). Analytical biochemistry. 1978;88(1):271-82.
49. Haghi M, van den Oetelaar W, Moir LM, Zhu B, Phillips G, Crapper J, et al. Inhalable tranexamic acid for haemoptysis treatment. European Journal of Pharmaceutics and Biopharmaceutics. 2015;93:311-9.
50. Nekrashevich S, Gritsenko V. Electronic structure of silicon dioxide (a review). Physics of the Solid State. 2014;56:207-22.
51. Kaialy W, Larhrib H, Chikwanha B, Shojaee S, Nokhodchi A. An approach to engineer paracetamol crystals by antisolvent crystallization technique in presence of various additives for direct compression. International journal of pharmaceutics. 2014;464(1-2):53-64.
52. Mohamed GG, Frag EY, Sedeek AA. Spectrophotometric methods for determination of tranexamic acid and etamsylate in pure form and pharmaceutical formulation. Insight Pharmaceutical Sciences. 2015;5:1-7.
53. Kane Z, Picetti R, Wilby A, Standing JF, Grassin-Delyle S, Roberts I, et al. Physiologically based modelling of tranexamic acid pharmacokinetics following intravenous, intramuscular, sub-cutaneous and oral administration in healthy volunteers. European Journal of Pharmaceutical Sciences. 2021;164:105893.
54. Moghrabi FS, Fadda HM. Drug Physicochemical Properties and Capsule Fill Determine Extent of Premature Gastric Release from Enteric Capsules. Pharmaceutics. 2022;14(11).
55. Gueche YA, Sanchez-Ballester NM, Bataille B, Aubert A, Rossi J-C, Soulairol I. Investigating the potential plasticizing effect of di-carboxylic acids for the manufacturing of solid oral forms with copovidone and ibuprofen by selective laser sintering. Polymers. 2021;13(19):3282.
56. Lu Z, Fassihi R. Influence of colloidal silicon dioxide on gel strength, robustness, and adhesive properties of diclofenac gel formulation for topical application. AAPS PharmSciTech. 2015;16:636-44.
57. Iqbal FM, Ahmad M, Tulain UR. Microwave radiation induced synthesis of hydroxypropyl methylcellulose-graft-(polyvinylalcohal-co-acrylic acid) polymeric network and its in vitro evaluation. Acta Poloniae Pharmaceutica. 2017;74(2):527-41.
58. Rahma A, Munir MM, Prasetyo A, Suendo V, Rachmawati H. Intermolecular interactions and the release pattern of electrospun curcumin-polyvinyl (pyrrolidone) fiber. Biological and Pharmaceutical Bulletin. 2016;39(2):163-73.
59. Zhao M, Barker SA, Belton PS, McGregor C, Craig DQ. Development of fully amorphous dispersions of a low Tg drug via co-spray drying with hydrophilic polymers. European Journal of Pharmaceutics and Biopharmaceutics. 2012;82(3):572-9.
60. Moynihan HA, O'Hare IP. Spectroscopic characterisation of the monoclinic and orthorhombic forms of paracetamol. International journal of pharmaceutics. 2002;247(1-2):179-85.

61. El Aita I, Breitkreutz J, Quodbach J. On-demand manufacturing of immediate release levetiracetam tablets using pressure-assisted microsyringe printing. European Journal of Pharmaceutics and Biopharmaceutics. 2019;134:29-36.
62. Qi S, Zhang B, McDonagh T. Three-dimensional Printed Implantable Products. Implantable Technologies2021. p. 252-95.